electronics

Article

Hybrid Reaching Law of Sliding Mode Position-Sensorless Speed Control for Switched Reluctance Motors

Seungyun Park [1], Jaepil Ban [1,2,*] and Suyoung Doh [3]

[1] School of Electronic Engineering, Kumoh National Institute of Technology, Gumi 39177, Republic of Korea; psy2080@kumoh.ac.kr
[2] Department of Aeronautic, Mechanical and Electronic Convergence Engineering, Kumoh National Institute of Technology, Gumi 39177, Republic of Korea
[3] Research Institute, NUC Electronics, Daegu 41548, Republic of Korea; dksgid@nuc.co.kr
* Correspondence: jpban@kumoh.ac.kr

Abstract: This study presents a method to reduce the chattering phenomenon and the reaching time of sliding mode speed control for switched reluctance motors (SRMs). In order to simultaneously reduce the chattering phenomenon and reaching time, we propose a hybrid reaching law (HRL) for sliding mode controller (SMC). Furthermore, to address the absence of a position sensor, a sliding mode observer (SMO) is integrated into the proposed HRL-based SMC, enabling accurate estimation of rotor angle and angular speed. Comprehensive simulation results are conducted to verify the effectiveness of the proposed method in terms of the reduced chattering phenomenon and reaching time.

Keywords: chattering phenomenon; electric motors; position and speed estimation; sliding mode control; switched reluctance motors

Academic Editor: Andrea Bonci

Received: 16 December 2024
Revised: 17 January 2025
Accepted: 27 January 2025
Published: 31 January 2025

Citation: Park, S.; Ban, J.; Doh, S. Hybrid Reaching Law of Sliding Mode Position-Sensorless Speed Control for Switched Reluctance Motors. *Electronics* **2025**, *14*, 577. https://doi.org/10.3390/electronics14030577

1. Introduction

Switched reluctance motors (SRMs) have attracted considerable attention in recent years across various fields, including aerospace, medical equipment, and energy-efficient home appliances, due to their advantages such as permanent magnet-free design, reduced manufacturing costs, simplified motor structure, wide speed range, and high reliability [1,2]. Despite the simplicity of their operation, SRMs present control challenges such as the presence of torque ripple and time-varying inductance property. To overcome these shortcomings, many control methods for SRMs have been conducted, including sliding mode control (SMC) [3–5], adaptive control [6–8], and torque-sharing function control [9,10]. Among these methods, SMC offers the advantage of ensuring control performance and system stability even in the presence of model uncertainties or disturbances.

SMC basically includes switching gains, which achieve robustness to uncertainties and determine the speed at which the states converge to the sliding surface. However, when the switching gain of SMC increases, a severe chattering phenomenon can be caused. One popular method to reduce the chattering phenomenon is to replace the switching function with a saturated function [11,12]. Another method is to add a boundary layer to the sliding surface [13]. This method ensures that all trajectories begin only within the boundary layer by defining the vicinity of the sliding surface as the boundary layer. In [14], intelligent complementary SMC was developed using an adaptive learning algorithm to estimate the lumped uncertainty. In [15], an arbitrary-order SMC was proposed for uncertain single-input single-output minimum-phase nonlinear systems. In [16], the switching control signal of the terminal sliding mode observer (SMO) was softened by a low-pass filter.

In [17], an enhanced exponential reaching law for variable-speed direct-driven wind energy conversion systems was proposed to reduce the chattering issue. In [18], in order to quicken the response of the sliding mode control system, a reaching law combining the exponential and power reaching law was proposed. In [19], a reaching law combined with extended state observer was proposed in order to optimize the permanent magnet synchronous motor (PMSM) speed regulation system and reduce the chattering phenomenon. While these methods can effectively mitigate the chattering phenomenon, it comes at the cost of a slower reaching time to the sliding surface or a complex control structure.

Meanwhile, to effectively operate SRMs, an accurate position sensor is essential for applying advanced control methods such as torque ripple minimization. However, as the resolution of sensors increases, their cost can also significantly rise, making it impractical to use high-quality sensors. In many industrial fields, the high cost of sensors not only increases the overall cost of SRM drives but also requires sufficient space for sensor installation, thereby increasing the volume of the motor and the complexity of the system. Consequently, to overcome these drawbacks, various sensorless algorithms have been studied [20,21]. For example, in [20], the second-order generalized integrator-based frequency-locked loop was used to estimate the rotor's angular velocity, and the active disturbance rejection control-based phase-locked loop was used to estimate the rotor's position, improving the system's robustness under the external perturbation and the dynamic performance of the system. Ref. [21] adopted SMO using a nonlinear polynomial flux linkage model to reduce computation cost. However, these methods can be too complex to design their controllers.

In this study, we propose a hybrid reaching law (HRL) for the sliding mode speed control of SRMs to achieve two conflicting objectives: reducing the chattering phenomenon and shortening the reaching time. Specifically, the HRL is newly designed for SRMs by jointly using terminal reaching and exponential-plus-proportional rate reaching terms. This newly designed HRL can simultaneously reduce the chattering phenomenon and the reaching time, regardless of load torque disturbances. Furthermore, to enable sensorless operation of the SRMs, the proposed SMC incorporates an SMO to accurately estimate the rotor's angle and angular speed. This integration of the SMO ensures the robustness of the system against parameter variations, as both the control and estimation methods are insensitive to the model uncertainties and external disturbances. Comprehensive simulation results demonstrate that the proposed HRL-based SMC outperforms the conventional SMC in terms of reduced chattering phenomenon and reaching time, under the various types of load torque disturbances. Additionally, the proposed control method maintains its efficacy when integrated with the SMO, ensuring reliable speed regulation even with the use of estimated rotor angle and angular speed. The main contributions of this study are summarized as follows:

1. The study proposes an HRL-based SMC method for the speed control of SRMs, with the aim of simultaneously reducing the chattering phenomenon and the reaching time to the sliding surface.
2. To facilitate sensorless operation, the proposed SMC method integrates an SMO that accurately estimates the rotor's angle and angular speed, ensuring the robustness of the speed control system against model uncertainties and external disturbances.
3. The stability and convergence properties of the proposed SMC and SMO are analyzed, yielding the conditions of parameters that ensure the stability and convergence of both the SMC and SMO.
4. Comprehensive simulations are conducted to demonstrate the effectiveness of the proposed HRL-based SMC method in terms of reduced chattering and reaching time,

and maintain its efficacy when integrated with the SMO for reliable speed regulation using estimated rotor angle and angular speed.

The remainder of this article is organized as follows. Section 2 illustrates the dynamic model of the switched reluctance motor and presents the conventional SMC method. Section 3 presents the proposed HRL-based SMC method integrated with an SMO. Simulation results are provided in Section 4, followed by the conclusion.

2. Preliminaries

2.1. Dynamic Model of Switched Reluctance Motors

According to the mechanical principles of the SRMs, the mechanical motion equations of the SRMs can be represented as follows [4]:

$$\dot{\theta} = \omega, \tag{1a}$$

$$\dot{\omega} = -\frac{b}{J}\omega + \frac{1}{J}T_e - \frac{1}{J}T_L, \tag{1b}$$

where θ is the rotor's angular position; ω is the rotor's angular speed; b and J are viscous frictional coefficients and the moment of inertia, respectively; T_e and T_L are the electromagnetic and load torques, respectively. In practice, it can be assumed that the magnitude of the load torque is bounded: $|T_L| \leq \beta$, where β is a positive constant. The electrical dynamics of SRMs can be represented as:

$$\dot{\psi}_k(i_k, \theta) = V_k - i_k R_k, \tag{2}$$

where ψ_k, V_k, i_k, and R_k are phase flux linkage, phase voltage, phase current, and phase resistance, respectively, for phase $k \in \{a, b, c\}$. By the integration of (2), we can obtain the flux linkage as:

$$\psi_k(i_k, \theta) = \int_0^t V_k(\tau) - i_k(\tau) R_k d\tau. \tag{3}$$

In this study, we assume that the phase currents are measured, but θ and ω are not measured.

2.2. Sliding Mode Speed Control of Switched Reluctance Motors

For considering speed control, we set the state variable model as follows:

$$x_1 = \theta - \theta^*, \tag{4a}$$

$$x_2 = \omega - \omega^*, \tag{4b}$$

where θ^* and ω^* are the reference position and speed of the rotor, respectively. Substituting (1), the time derivative of (4) can be obtained as:

$$\dot{x}_1 = \omega - \omega^* = x_2, \tag{5a}$$

$$\dot{x}_2 = \dot{\omega} = \frac{1}{J}(T_e - b\omega - T_L). \tag{5b}$$

From (5), we have

$$\begin{aligned} \dot{x}_2 &= -\frac{b}{J}(x_2 + \omega^*) + \frac{1}{J}T_e - \frac{T_L}{J} \\ &= -\frac{b}{J}x_2 + \frac{1}{J}(T_e - b\omega^*) - \frac{T_L}{J}. \end{aligned} \tag{6}$$

By defining $u = T_e - b\omega^*$, the state equation from (6) can be defined as follows:

$$\begin{cases} \dot{x}_1 = x_2 \\ \dot{x}_2 = Ax_2 + B(u - T_L), \end{cases} \quad (7)$$

where $A = -b/J$, $B = 1/J$. In addition, the sliding surface is given by:

$$s = x_2 + \eta x_1, \quad (8)$$

where $\eta > 0$ is a constant. In SMC, the reaching law is designed to track the sliding surface, ensuring the control system achieves stable conditions. The following represents a typical design of $\dot{s}$ in conventional constant-plus-proportional reaching law (CPRL) [22].

$$\dot{s} \ = \ -\epsilon\text{sign}(s) \ - \lambda s, \quad (9)$$

where s represents the sliding surface, and $\text{sign}(s)$ represents the constant reaching term. λ represents the proportional rate term.

Note that the reaching time to the sliding surface can be reduced by increasing the value of the parameter ϵ. However, the sign function in the control law induces a chattering phenomenon, with larger values of ϵ leading to increased chattering effects. Consequently, there is a trade-off between achieving a reduced reaching time and the chattering effect. Thus, the goal of this study is to design a novel reaching law-based SMC method that can simultaneously achieve an effectively reduced reaching time and the chattering phenomenon in position-sensorless SRMs.

3. Main Results

3.1. Overview of the Proposed Method

Figure 1 shows the overall diagram of the proposed method. The control inputs and current measurements are used in the SMO-based position and speed estimator to obtain the estimates of rotor position and speed. The error between the estimated speed $\hat{\omega}$ and reference speed ω^* is then applied to the HRL-based SMC, generating the current reference i_{ref}. A hysteresis current controller is used for the phase current control, generating gate switching signals to drive the SRMs using a half-bridge asymmetric converter. In the following subsections, we present the details on the proposed HRL-based SMC with SMO-based position and speed estimation, along with their stability and convergence analyses.

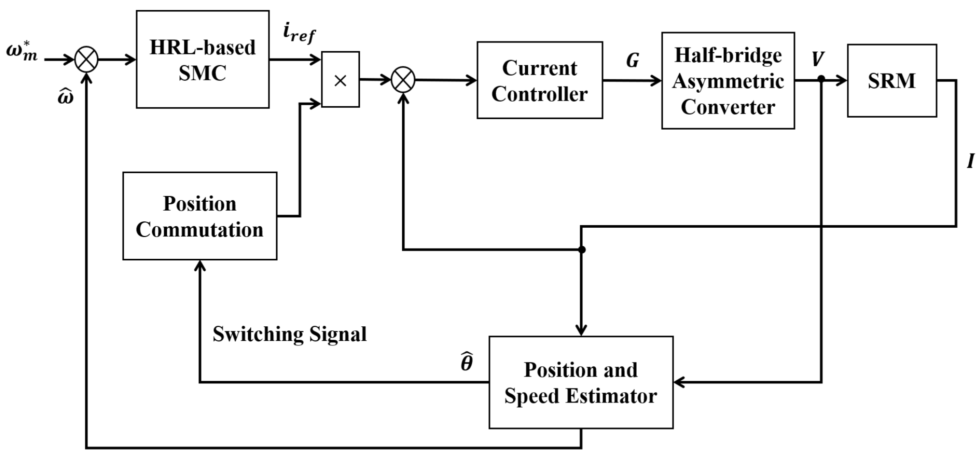

Figure 1. Overall diagram of proposed HRL-based SMC.

3.2. Hybrid Reaching Law

We design the time-derivative of a sliding surface s for the proposed HRL as follows:

$$\dot{s} = -m|x_1|^a s - \frac{c}{k}\left(e^{k|x_1|} - 1\right)s, \tag{10}$$

where $a > 0$, $m > 0$, $c > 0$, and $0 < k < 1$.The proposed HRL consists of two parts: $-m|x_1|^a s$, the terminal reaching part, and $-\frac{c}{k}(e^{k|x_1|} - 1)s$, the exponential plus proportional rate reaching part. As the state variable x_1 included in the reaching law, the reaching time depends on the magnitude of the state. For example, if $|x_1|$ is large, it means that the system's state variable is far away from the origin. In this case, if we increase the reaching coefficient enough, then the convergence process can be accelerated. On the other hand, when the state variable of the system is relatively close to the origin, the reaching coefficient needs to be small to avoid undesirable chattering effects. Thus, the proposed HRL can effectively reduce the chattering phenomenon and achieve a reduced reaching time simultaneously. Specifically, large a and m reduce the reaching time. In addition, as a increases, the chattering phenomenon is reduced, while m has an opposite effect from that of a for reducing the chattering. Additionally, c and k marginally affect the reaching time, while large values of c and k reduce the chattering effect. Therefore, the parameters a, c, k, and m must be appropriately selected to effectively reduce the reaching time and the chattering phenomenon according to the above guideline.

Now, we derive the control input u for designing $\dot{s}$ as (10). Taking the time-derivative of the sliding surface (8) yields

$$\dot{s} = \dot{x}_2 + \eta \dot{x}_1. \tag{11}$$

Substituting (7) into (11) with $T_L = 0$, we have

$$\dot{s} = (A + \eta)x_2 + Bu. \tag{12}$$

Now, we want to design $\dot{s}$ as in (10) using the control input u. Using (10) and (12), the input u is derived as follows:

$$\begin{aligned} (A+\eta)x_2 + Bu &= -m|x_1|^a s - \frac{c}{k}\left(e^{k|x_1|} - 1\right)s \\ \Longleftrightarrow Bu &= -m|x_1|^a s - \frac{c}{k}\left(e^{k|x_1|} - 1\right)s - (A+\eta)x_2 \\ \Longleftrightarrow u &= \frac{1}{B}\left[-m|x_1|^a s - \frac{c}{k}\left(e^{k|x_1|} - 1\right)s - (A+\eta)x_2\right]. \end{aligned} \tag{13}$$

Furthermore, the input torque T_e can be obtained as follows by $u = T_e - b\omega^*$:

$$T_e = \frac{1}{B}\left[-m|x_1|^a s - \frac{c}{k}\left(e^{k|x_1|} - 1\right)s - (A+\eta)x_2\right] + b\omega^*. \tag{14}$$

Since torque can be converted into current (6), the reference current input is written as in [23]:

$$i_{\text{ref}} = \sqrt{KT_e}, \tag{15}$$

where K is constant. The operation of SRMs requires each phase current to be applied from the unaligned position to the aligned position. Thus, during the period when the phase current is applied, $dL(\theta)/d\theta$ can be considered constant, implying that K is constant. The flowchart of the proposed HRL-based SMC is shown in Figure 2.

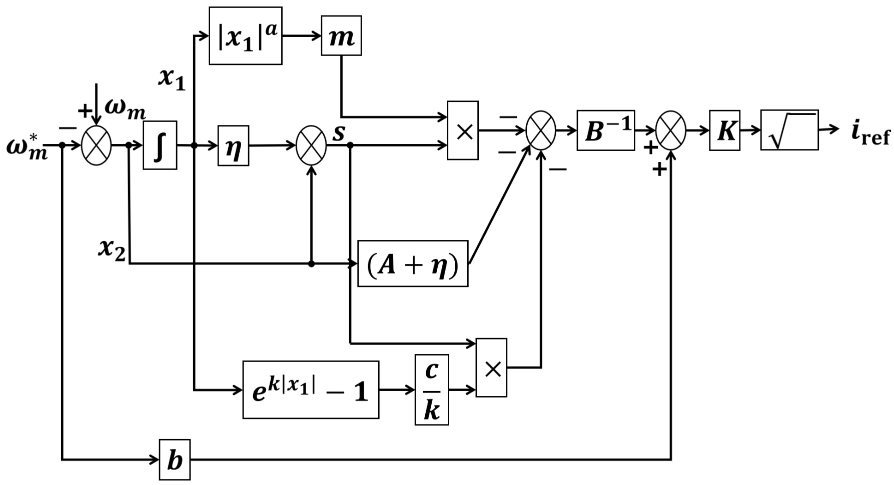

Figure 2. Flowchart of the variable structure of the system parameter i_{ref}.

3.3. Stability Analysis of the Proposed SMC

The proposed HRL-based SMC is initially developed under the assumption that the load torque T_L is equal to zero. To ensure the validity of the proposed method in more practical scenarios where $T_L \neq 0$, we present a detailed stability analysis to verify the robustness of the control system. Define the Lyapunov function candidate as:

$$V(x) = \frac{1}{2}s^2. \tag{16}$$

The time derivative of (16) can be obtained as:

$$\begin{aligned} \dot{V} &= s\dot{s} = s(\dot{x}_2 + \eta\dot{x}_1) \\ &= s\{(A+\eta)x_2 + Bu - BT_L\}. \end{aligned} \tag{17}$$

Substituting (13) into (17) yields

$$\begin{aligned} \dot{V} &= s\left\{-m|x_1|^a s - \frac{c}{k}\left(e^{k|x_1|} - 1\right)s - BT_L\right\} \\ &\leq -m|x_1|^a s^2 - \frac{c}{k}\left(e^{k|x_1|} - 1\right)s^2 + B|s||T_L| \\ &\leq -m|x_1|^a s^2 - \frac{c}{k}\left(e^{k|x_1|} - 1\right)s^2 + B\beta|s| \\ &= -|s|\left(\left\{m|x_1|^a + \frac{c}{k}\left(e^{k|x_1|} - 1\right)\right\}|s| - B\beta\right) < 0 \\ &\quad \forall |s| > \rho. \end{aligned} \tag{18}$$

where $\rho > \frac{\beta B}{m|x_1|^a + \frac{c}{k}(e^{k|x_1|}-1)}$ $\forall |x_1| > 0$. Therefore, s is ultimately bounded. If $T_L = 0$, β is zero. Then, s is asymptotically stable as $\dot{V} < 0$ $\forall s \neq 0$.

3.4. SMO-Based Rotor Position and Speed Estimation

Figure 3 illustrates the overall diagram of SMO-based position and speed estimation. The phase flux linkage is calculated based on the SRM model using phase current, voltage, and resistance. Then, the estimation of phase flux linkage is obtained using flux observer. Finally, the sliding mode observer estimates the speed and position of rotors using the flux linkage estimation errors.

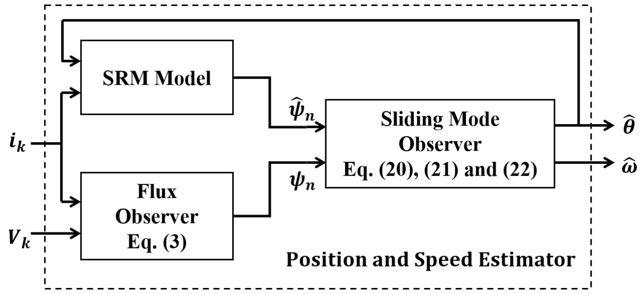

Figure 3. Block diagram of the sliding mode observer.

The sliding mode observer for estimating θ and ω is constructed as follows:

$$\dot{\hat{\theta}} = \hat{\omega} + k_\theta \text{sgn}(e_f) \tag{19a}$$

$$\dot{\hat{\omega}} = k_\omega \text{sgn}(e_f), \tag{19b}$$

where $\hat{\theta}$ and $\hat{\omega}$ are the rotor's estimated angle and angular speed, respectively; e_f is an error function based on measured and estimated variables. There are many possible error functions available. According to [24], the error function can be selected as follows:

$$e_f = \sum_{n=1}^{N_{ph}} f_n'(\hat{\theta})(\psi_n - \hat{\psi}_n) \text{ with } f_n' = \frac{df_n}{d\theta}\bigg|_{\theta=\hat{\theta}}, \tag{20}$$

where $f_n(\theta) = \cos(N_r\theta - (n-1)2\pi/N_{ph})$. Here, N_r and N_{ph} are the numbers of the rotor and stator poles, respectively; the estimated flux linkage $\hat{\psi}_n(i_k, \hat{\theta}_k)$ can be identified and stored in a lookup table.

Now, we present the convergence analysis of the estimation error of the SMO. Define the estimation error as:

$$e_\theta = \theta - \hat{\theta} \tag{21a}$$

$$e_\omega = \omega - \hat{\omega}. \tag{21b}$$

We assume that there exist γ such that $|e_\omega| \leq \gamma$. This assumption is valid in practice because the speed of the motor is bounded, and the bound can be readily obtained. By the time derivative of (21a), we have

$$\begin{aligned} \dot{e}_\theta &= \dot{\theta} - \dot{\hat{\theta}} \\ &= \omega - \hat{\omega} - k_\theta \text{sgn}(e_f) \\ &= e_\omega - k_\theta \text{sgn}(e_f). \end{aligned} \tag{22}$$

On the other hand, the time derivative of (21b) yields

$$\begin{aligned} \dot{e}_\omega &= \dot{\omega} - \dot{\hat{\omega}} \\ &= -\frac{b}{J}\omega + \frac{1}{J}(T_e - T_L) - k_\omega \text{sgn}(e_f) \end{aligned} \tag{23}$$

If k_ω is selected large enough, the first and second term of (23) can be neglected [25]. Thus, (23) can be obtained as:

$$\dot{e}_\omega = -k_\omega \text{sgn}(e_f) \tag{24}$$

Now, we consider the Lyapunov function candidate $V = V_1 + V_2$, where $V_1 = \frac{1}{2}e_\theta^2$ and $V_2 = \frac{1}{2}e_\omega^2$. By the time derivative of V_1, we have:

$$\begin{aligned}\dot{V}_1 &= e_\theta \dot{e}_\theta \\ &= e_\theta \Big(e_\omega - k_\theta \text{sgn}(e_f) \Big)\end{aligned} \tag{25}$$

According to [26], sgn(e_f) = sgn(e_θ). Thus, (25) is represented as follows:

$$\begin{aligned}\dot{V}_1 &= e_\theta (e_\omega - k_\theta \text{sgn}(e_\theta)) \\ &\leq -|e_\theta|(k_\theta - |e_\omega|) \quad (26) \\ &\leq -|e_\theta|(k_\theta - \gamma) < 0 \quad \forall k_\theta > \gamma. \quad (27)\end{aligned}$$

Therefore, we can conclude that e_θ converges to zero. On the other hand, the time derivative of V_2 can be calculated as:

$$\begin{aligned}\dot{V}_2 &= e_\omega \dot{e}_\omega \\ &= e_\omega \Big(-k_\omega \text{sgn}(e_f) \Big).\end{aligned} \tag{28}$$

In addition, when e_θ converges to zero, $\dot{e}_\theta$ also converges to zero. Therefore, we have from (22):

$$0 = e_\omega - k_\theta \text{sgn}(e_f). \tag{29}$$

By substituting (29) into (28), one can obtain:

$$\begin{aligned}\dot{V}_2 &= e_\omega \left(-\frac{k_\omega}{k_\theta} e_\omega \right) \\ &= -e_\omega^2 \left(\frac{k_\omega}{k_\theta} \right) < 0.\end{aligned} \tag{30}$$

Therefore, we have $\dot{V} = \dot{V}_1 + \dot{V}_2 < 0$ if we choose $k_\theta \geq \gamma$ and $k_\theta > 0$ [27].

4. Simulation Results

In this section, comprehensive case studies are presented to verify the effectiveness of the proposed method. MATLAB/Simulink 2024a was used for conducting simulations. Table 1 presents the detailed specifications of the SRMs considered in the simulations. To fully illustrate the performance of the proposed method, a comparison analysis was conducted with the recently published hybrid reaching law in [28] (conv. 1) and conventional CPRL-based SMC method (conv. 2). For convenience, we recall the reaching law of conv. 1 as follows:

$$\dot{s} = -A_1|x_2|^{a_1}s - A_2|x_2|^{a_2}\text{sign}(s). \tag{31}$$

The parameters for the conv. 1 method were chosen as follows: $A_1 = 168$, $A_2 = 250$, $a_1 = 0.6$, $a_2 = 1$. The parameters for the conv. 2 method were chosen as follows: $\epsilon = 500$, $\lambda = 300$. The parameters of the proposed method were selected $m = 700$, $a = 1$, $c = 1$, $k = 0.05$, $\eta = 1$, $K = 2$, $k_\theta = 5$, and $k_\omega = 5000$. The sampling time of the simulation was set as 10 µs. The value of the upper bound of T_L of all simulations was set not to exceed 0.015 N·m.

Table 1. Specification of SRMs in the simulation.

Parameters	Symbols	Values
Resistance	R	2 [Ω]
Inertial	J	2.66×10^{-5} [kgm^2]
Friction	b	2.44×10^{-5} [N·m·s]
Voltage	V_{dc}	24 [V]
Maximum Current	I_{max}	3 [A]
Initial Speed	ω_0	$2000\pi/30$ [rad/s]

4.1. Speed Tracking Performance

Figure 4 illustrates the speed tracking results by the proposed and conventional method. The reference speed ω_{ref} was set to 2000 rpm for $t = 1$ s and then increased by 250 rpm in steps every 0.5 s thereafter, eventually reaching a final reference speed of 4000 rpm. Additionally, the load torque was set to 0.005 N·m. The proposed method exhibited faster tracking response than that of conv. 1 and conv. 2. Figures 4 and 5, respectively, show the speed tracking trajectories and tracking errors of the proposed and conventional methods. It is clear that the conventional methods exhibited large deviations from the reference speed, whereas the speed controlled by the proposed method exhibited the faster response, implying that the proposed method outperformed the conventional methods in terms of the reference tracking. Table 2 represents the integral square error (ISE) and integral absolute error (IAE) values for the speed tracking errors obtained using the proposed and conventional methods. The results show that the proposed method achieved 4.23%, 57.93% reduction in ISE and 32.94%, 53.67% reduction in IAE, compared to the conv. 1 and conv. 2 methods, respectively. Figure 6 shows the trajectory of s. The sliding variable s of the proposed method reaches the sliding surface ($s = 0$) faster than those of the conventional methods. Furthermore, the reaching time of proposed method is smaller than those of the conventional methods. Figure 7 illustrates the chattering phenomenon by the proposed and the conventional methods. As we can see from the result, the magnitudes of chattering by the proposed and conv. 1 and conv. 2 methods were 5.94, 6.38, and 7.98. The proposed method exhibited 14.29% and 25.56% reduction in chattering compared to the conv.1 and conv.2 methods, respectively.

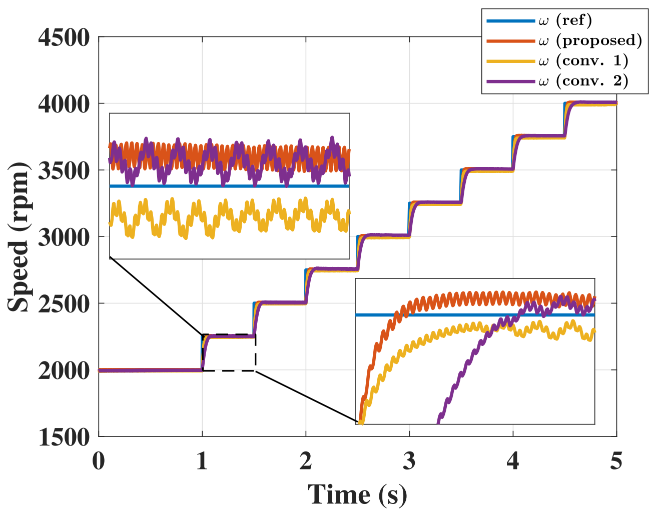

Figure 4. Trajectories of speed controlled by the proposed and conventional methods with a step reference change.

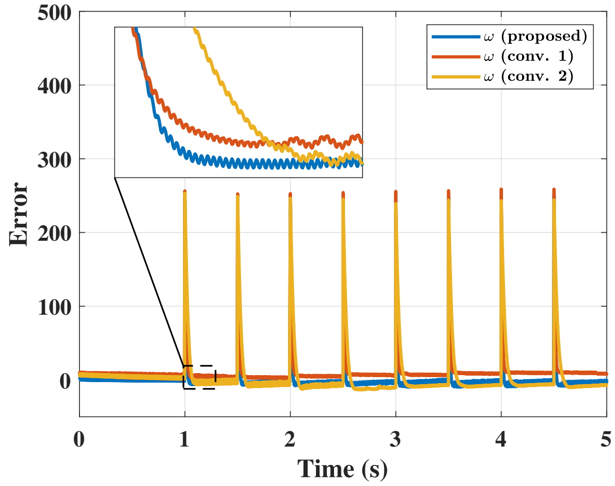

Figure 5. Speed tracking error (ω_{ref}) by the proposed and conventional methods.

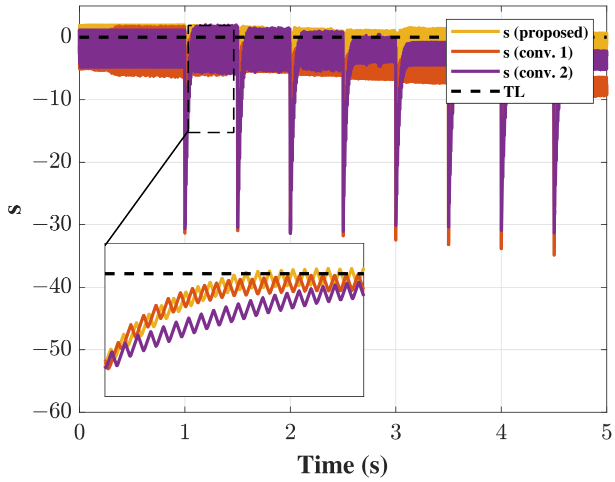

Figure 6. Trajectories of s of the proposed and conventional methods.

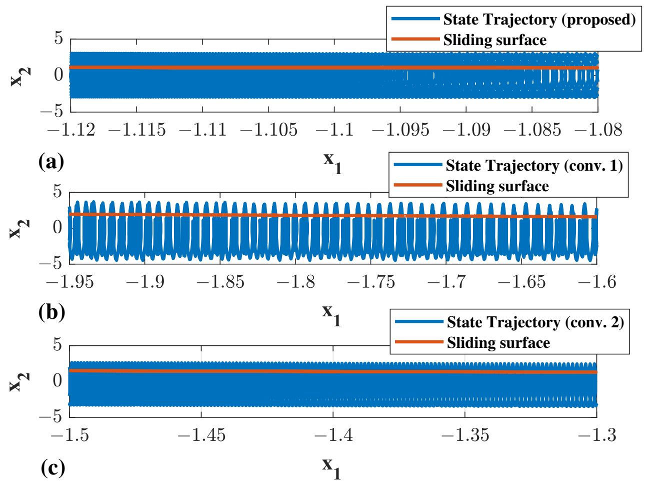

Figure 7. Comparison of chattering phenomenon between (**a**) proposed, (**b**) conv. 1 and (**c**) conv.2 methods.

Table 2. ISE and IAE for the tracking error by the proposed and conventional methods.

	Proposed	Conv. 1	Conv. 2
ISE	16.1663	16.8805	38.4262
IAE	1.8618	2.7765	4.0182

4.2. Effect of Step Load Torque Variations

Figure 8 shows the speed regulation results of the proposed and conventional methods for step changes in load torque. The load torque T_L was set to 0.005 N·m from $t = 0$ to $t = 0.5$ s and decreased to 0 N·m from $t = 0.5$ s to $t = 1.5$ s. This process was repeated for $t = 5$ s. The results show that the proposed method can effectively follow the reference speed despite the sudden change in the load torque, whereas the conventional methods failed to accurately follow the reference speed and exhibited a constant steady-state error under the same load torque. Table 3 shows that the proposed method achieved a 20.61%, 47.18% reduction in ISE and a 26.14%, 39.32% reduction in IAE, compared to those of the conv. 1 and conv. 2 methods, respectively.

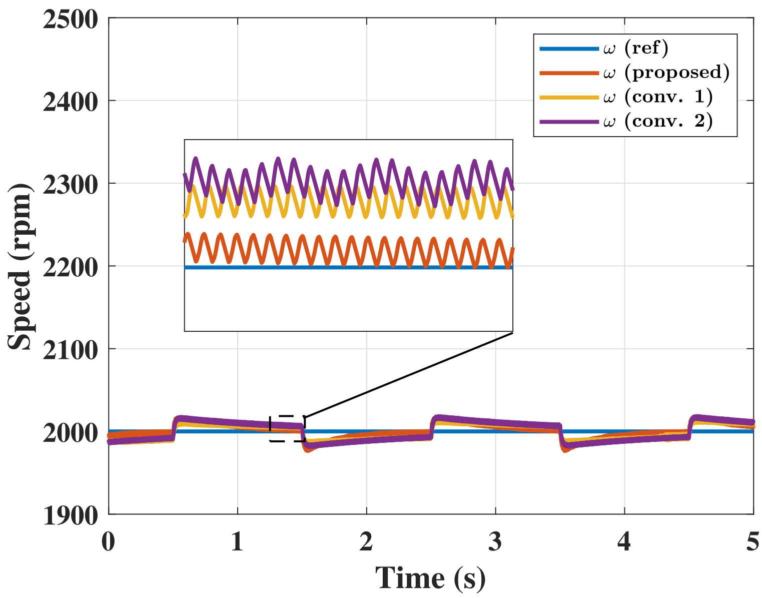

Figure 8. Trajectories of rotor speed under step load torque changes.

Table 3. ISE and IAE for the tracking error by the proposed and conventional methods under the step load torque changes.

	Proposed	Conv. 1	Conv. 2
ISE	1.9560	2.4638	3.7032
IAE	1.7757	2.4040	2.9264

4.3. Effect of Continuous Load Variations

In this subsection, the speed regulation results of the proposed method are evaluated under continuous load variations. The load torque T_L was set to vary continuously following a sinusoidal wave with an amplitude of 0.0025 N·m, a frequency of π, and a bias of 0.005 N·m. The results demonstrate that the deviation from the desired speed by the proposed method was smaller than those of the conventional methods (Figure 9). Table 4 shows that the proposed method achieved 24.25%, 56.07% reduction in ISE and 8.51%, 33.02% reduction in IAE, compared to those of the conv. 1 and conv. 2 methods, respectively.

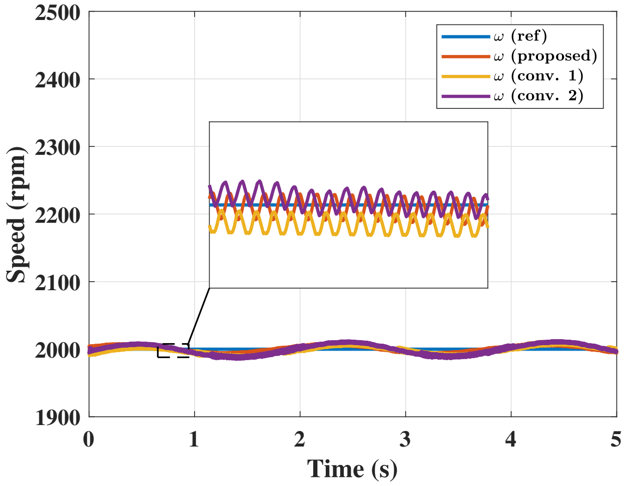

Figure 9. Trajectories of rotor speed under the continuous load torque change.

Table 4. ISE and IAE for the tracking error by the proposed and conventional methods under the continuous load torque change.

	Proposed	Conv. 1	Conv. 2
ISE	0.6654	0.8784	1.5147
IAE	1.1455	1.2520	1.7102

4.4. Effect of Complex Load Variations

In this subsection, the performance of the proposed method is evaluated under complex load variations. The load torque T_L was set to vary in both continuous and step, where the sine wave and step load torque were set to the same conditions as those in Sections 4.2 and 4.3. Figure 10 demonstrates that the proposed method exhibited relatively smaller regulation errors compared to conventional methods. Furthermore, when a disturbance was applied, the proposed method recovered the desired speed more quickly than conventional methods. Table 5 shows that the proposed method achieved 75.26%, 80.34% reduction in ISE and 51.45%, 55.16% reduction in IAE, compared to those of the conv. 1 and conv. 2 methods, respectively.

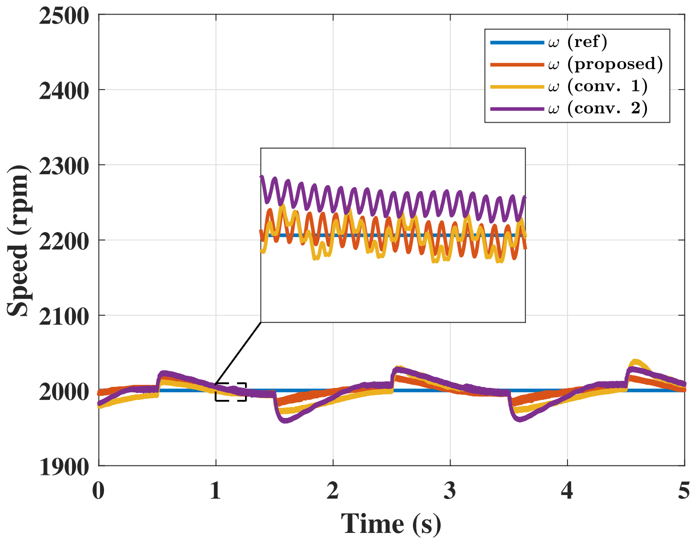

Figure 10. Trajectories of rotor speed under the complex load torque changes.

Table 5. ISE and IAE for the tracking error by the proposed and conventional methods under the complex load torque changes.

	Proposed	**Conv. 1**	**Conv. 2**
ISE	1.5074	6.0931	7.6655
IAE	1.5083	3.1065	3.3635

5. Conclusions

In this study, a position-sensorless HRL-based SMC method was proposed for speed control of SRMs. The proposed method was designed by incorporating a state variable into the reaching coefficient of SMC to reduce chattering and reaching time simultaneously. In order to estimate the rotor's angle and angular speed, an SMO was adopted to make the position and speed estimation robust to the load torque variations. The stability and convergence analysis for the proposed controller and observer were conducted to derive the conditions for appropriately choosing controller and observer gains. Comprehensive simulation studies were conducted for various conditions characterized by changes in speed references and load torques. The simulation results verified that the proposed method reduced the chattering phenomenon and reaching time simultaneously compared to the conventional methods. Experimental validation accounting for model uncertainties is identified as a direction for future work.

Author Contributions: Conceptualization, Software, Validation, Methodology: S.P. and J.B.; Formal analysis and Investigation: S.P.; Writing—original draft, S.P.; Writing—review and editing: S.P., J.B. and S.D.; Funding acquisition and Supervision: J.B.; Resources: S.D. All authors have read and agreed to the published version of the manuscript.

Funding: Following are results of a study on the "Leaders in INdustry-university Cooperation 3.0" Project, supported by the Ministry of Education and National Research Foundation of Korea.

Data Availability Statement: Data are contained within the article.

Conflicts of Interest: The authors declare no conflicts of interest.

References

1. Wang, X.; Palka, R.; Wardach, M. Nonlinear digital simulation models of switched reluctance motor drive. *Energies* **2020**, *13*, 6715
2. Watthewaduge, G.; Bilgin, B. Reluctance mesh-based magnetic equivalent circuit modeling of switched reluctance motors for static and dynamic analysis. *IEEE Trans. Transp. Electrif.* **2022**, *8*, 2164–2176. [CrossRef]
3. Scalcon, F.P.; Fang, G.; Vieira, R.P.; Grundling, H.A.; Emadi, A. Discrete-time super-twisting sliding mode current controller with fixed switching frequency for switched reluctance motors. *IEEE Trans. Power Electron*. **2022**, *37*, 3321–3333. [CrossRef]
4. Yin, Y. Optimal Direct Instantaneous Torque Control for SRMs Using Advanced Sliding Mode Controller. *Appl. Sci*. **2022**, *12*, 12177. [CrossRef]
5. Vinh, V.Q.; Ha, V.T. Improved torque ripple of switched reluctance motors using sliding mode control for electric vehicles. *Eng. Technol. Appl. Sci. Res.* **2023**, *13*, 10140–10144. [CrossRef]
6. Masoudi, S.; Soltanpour, M.R.; Abdollahi, H. Adaptive fuzzy control method for a linear switched reluctance motor. *IET Electr. Power. Appl*. **2018**, *12*, 1328–1336. [CrossRef]
7. Masoudi, S.; Mehrjerdi, H.; Ghorbani, A. Adaptive control strategy for speed control of a linear switched reluctance motor. *IET Electr. Power Appl*. **2020**, *14*, 1496–1503. [CrossRef]
8. Al-Amyal, F.; Hamouda, M.; Szamel, L. Performance improvement based on adaptive commutation strategy for switched reluctance motors using direct torque control. *Alex. Eng. J.* **2022**, *61*, 9219–9233. [CrossRef]
9. Ye, W.; Ma, Q.; Zhang, P. Improvement of the Torque-Speed Performance and Drive Efficiency in an SRM Using an Optimal Torque Sharing Function. *Appl. Sci*. **2018**, *8*, 750. [CrossRef]
10. Huang, C.; Cao, W.; Xu, J. An NUTSF at Sub-Region for Suppression of Torque Ripple in Switched Reluctance Motors. *Appl. Sci*. **2022**, *12*, 7604. [CrossRef]

11. Aguilar-Ibañez, C. Stabilization of the PVTOL aircraft based on a sliding mode and a saturation function. *Int. J. Robust Nonlinear Control*. **2017**, *27*, 843–859. [CrossRef]
12. Zheng, C.; Hu, C.; Yu, J.; Wen, S. Saturation function-based continuous control on fixed-time synchronization of competitive neural networks. *Neural Netw.* **2024**, *169*, 32–43. [CrossRef] [PubMed]
13. Cupertino, F.; Naso, D.; Mininno, E.; Turchiano, B. Sliding-mode control with double boundary layer for robust compensation of payload mass and friction in linear motors. *IEEE Trans. Ind. Appl*. **2009**, *45*, 1688–1696. [CrossRef]
14. Lin, F.J.; Hwang, J.C.; Chou, P.H.; Hung, Y.C. FPGA-based intelligent-complementary sliding-mode control for PMLSM servo-drive system. *IEEE Trans. Power Electron*. **2010**, *25*, 2573–2587. [CrossRef]
15. Laghrouche, S.; Plestan, F.; Glumineau, A. Higher order sliding mode control based on integral sliding mode. *Automatica* **2007**, *43*, 531–537. [CrossRef]
16. Feng, Y.; Yu, X.; Han, F. High-order terminal sliding-mode observer for parameter estimation of a permanent-magnet synchronous motor. *IEEE Trans. Ind. Electron*. **2012**, *60*, 4272–4280. [CrossRef]
17. Mozayan, S.M.; Saad, M.; Vahedi, H.; Fortin-Blanchette, H.; Soltani, M. Sliding mode control of PMSG wind turbine based on enhanced exponential reaching law. *IEEE Trans. Ind. Electron*. **2016**, 63, 6148–6159. [CrossRef]
18. Han, Y.; Cheng, Y.; Xu, G. Trajectory tracking control of AGV based on sliding mode control with the improved reaching law. *IEEE Access*. **2019**, *7*, 20748–20755. [CrossRef]
19. Wang, Y.; Feng, Y.; Zhang, X.; Liang, J. A new reaching law for antidisturbance sliding-mode control of PMSM speed regulation system. *IEEE Trans. Power Electron*. **2019**, *35*, 4117–4126. [CrossRef]
20. Ni, F.; Zhang, W.; Bi, Y.; Li, B. The Study of SRM Sensorless Control Strategy Based on SOGI-FLL and ADRC-PLL Hybrid Algorithm. *Electronics* **2023**, *13*, 2. [CrossRef]
21. Peng, F.; Ye, J.; Emadi, A.; Huang, Y. Sensorless Control of Switched Reluctance Motor Based on Sliding Mode Observer Using Nonlinear Flux Linkage Model. In Proceedings of the 2023 26th International Conference on Electrical Machines and Systems (ICEMS), Zhuhai, China, 5–8 November 2023.
22. Sun, X.; Cao, J.; Lei, G.; Guo, Y.; Zhu, J. A Composite Sliding Mode Control for SPMSM Drives Based on a New Hybrid Reaching Law With Disturbance Compensation. *IEEE Trans. Transp. Electrif*. **2021**, *7*, 1427–1436.
23. Namazi, M.M.; Rashidi, A.; Koofigar, H.; Saghaiannejad, S.M.; Ahn, J.W. Adaptive control of switched reluctance motor drives under variable torque applications. *J. Electr. Eng. Technol.* **2017**, *12*, 134–144.
24. McCann, R.A.; Islam, M.S.; Husain, I. Application of a sliding-mode observer for position and speed estimation in switched reluctance motor drives. *IEEE Trans. Ind. Appl*. **2001**, *37*, 51–58.
25. Islam, M.S.; Husain, I.; Veillette, R.J.; Batur, C. Design and performance analysis of sliding-mode observers for sensorless operation of switched reluctance motors. *IEEE Trans. Control Syst. Technol.* **2003**, *11*, 383–389.
26. Husain, I.; Sodhi, S.; Ehsani, M. A sliding mode observer based controller for switched reluctance motor drives. *IEEE Ind. Appl. Soc. Annu. Meet.* **1994**, *1*, 635–643.
27. Jamil, M.U.; Kongprawechnon, W.; Chayopitak, N. Active fault diagnosis of a switched reluctance motor using sliding mode observer and average torque estimator for light electric vehicle applications. *Int. Trans. Electr. Energy Syst.* **2020**, *30*, 1–22.
28. Zhang, Z.; Liu, X.; Yu, J.; Yu, H. Time-varying disturbance observer based improved sliding mode single-loop control of PMSM drives with a hybrid reaching law. *IEEE Trans. Energy Convers.* **2023**, *38*, 2539–2549.